Results in Physics 10 (2018) 187–193

Contents lists available at ScienceDirect

Results in Physics

journal homepage: www.elsevier.com/locate/rinp

Mechanical properties of pre-strained austenitic stainless steel from the view of energy density

Jian Peng[a,c,*], Kaishang Li[a], Qiao Dai[b,c], Jian Peng[a]

[a] School of Mechanical Engineering, Changzhou University, Changzhou, Jiangsu 213164, China
[b] School of Mechanical Engineering, Jiangsu University of Technology, Changzhou, Jiangsu 213001, China
[c] Jiangsu Key Laboratory of Green Process Equipment, Changzhou University, Changzhou, Jiangsu 213164, China

ARTICLE INFO

Keywords:
Austenitic stainless steel
Pre-strain
Energy dissipation variable
Mechanical properties
Hollomon model

ABSTRACT

The effect of pre-strain on mechanical properties was investigated for 316L austenitic stainless steel over pre-strain value ranging from 0% to 35%. The effect of pre-strain on energy density of tensile curve was focused, and pre-strain enhances elastic energy density while reduces fracture energy density. Moreover, an energy dissipation variable was proposed based on fracture energy density as a damage parameter of pre-strained material. The relationships between energy dissipation variable and tensile mechanical properties were discussed. Finally, based on energy dissipation variable, an improved Hollomon model considering pre-strain damage is developed to predict mechanical properties of pre-strained 316L austenitic stainless steel.

Introduction

Due to the excellent ductility and relatively low yield strength of austenitic stainless steel, strain strengthening technology is used for pressure equipment with austenitic stainless steel to weight reduction. There is an urgent need to understand the effect of pre-strain on mechanical properties of austenitic stainless steel. Researchers paid attention to the effect of pre-strain on microstructural evolution [1–3] and macroscopic properties, such as hydrogen embrittlement [4–6], low-temperature carburization [7] and tensile strength [8]. Based on the effects of pre-strain and strain rate on dislocation, mechanical twinning and α'-martensite of 304L, Lee et al. [4] explained the variation of mechanical parameter with pre-strain and strain rate. Ji et al. [5] studied the effect of pre-strain on hydrogen embrittlement of 310S stainless steel and found that the pre-strain increased the resistance to hydrogen embrittlement by suppressing the fracture transition. The effect of pre-strain on low-temperature surface carburization of 304 austenitic stainless steel were studied by Peng et al. [7], and they found the carburized 304 stainless steel has an outstanding surface hardness with compressive residual stress, and the carburizing strengthening was independent of plastic pre-strain.

Besides microstructure and mechanical properties of materials, strain energy is an important parameter to understand physical properties of materials. Energy density was used to study tensile behavior [9,10], fatigue failure [11,12] and damage variable [13,14] of metallic materials. Lazzarin and Zambardi [10] re-formulated and applied the equivalent strain energy density approach to predict the stress intensity factors of V-shaped notch specimens on the basis of the linear elastic stress distribution. Koh [11] predicted the fatigue life of high pressure tube steel using cyclic strain energy density with a good correlation with the experimental life. Guu et al. [13] studied the effect of electrical discharge machining on surface characteristics and machining damage of AISI D2 tool steel, and they introduced strain energy density into damage variable to study the electrical discharge machining damage. Strain energy density is a useful parameter with physical meaning and can be applied for the analyses of mechanical parameters. Hollomon model was widely used to characterize the stress-strain curve of materials owing to its simplicity and effectiveness [15-19]. Zhang et al. [15] studied the effects of cold rolling on microstructure evolution and mechanical hardening of Inconel 690 alloy and used Hollomon model to describe stress-strain curves. Colla et al. [18] used Hollomon model to describe strain hardening behavior of dual-phase steels.

In order to understand mechanical properties of pre-strained 316L austenitic stainless steel from the view of energy density, strain energy density will be applied to analyze the variation laws of strength parameter and elongation parameter. Moreover, an energy dissipation variable, which reveals the damage evolution of pre-strained material with pre-strain, will be proposed based on damage theory and fracture energy density. At last, an improved Hollomon model based on the energy dissipation variable considering pre-strain damage will be constructed and applied to the pre-strained 316L austenitic stainless steel.

* Corresponding author at: School of Mechanical Engineering, Changzhou University, Changzhou, Jiangsu 213164, China.
E-mail address: joepengjian@163.com (J. Peng).

https://doi.org/10.1016/j.rinp.2018.05.034
Received 7 March 2018; Received in revised form 21 May 2018; Accepted 21 May 2018
Available online 30 May 2018

Table 1
Composition of 316L austenitic stainless steel (wt%).

Steel	C	Si	Cr	Fe	Ni	Mo	P	S	Mn
316L	0.03	0.55	18.52	68.50	9.06	1.46	0.03	0.02	1.83

Experiments and results

Experimental details

The as-received 316L austenitic stainless steel is hot-rolled steel plate with 3 mm thickness, and the composition is listed in Table 1. The average austenite grain size of the material is about 18 μm.

Tensile specimens shown in Fig. 1 were machined from as-received metallic plate with length 35 mm × width 6 mm × thickness 3 mm, which meet the testing standard of ASTM E8M-04 [20]. Tensile specimens were stress relief annealed at 753 K with 2 h. Then specimens were polished with 1500 grit emery papers to achieve the same surface roughness. In order study the effect of pre-strain on the mechanical properties of 316L austenitic stainless steel, as-received specimens and pre-strained specimens with eight pre-strain levels 4%, 8%, 12%, 16%, 20%, 24%, 28%, 35% were considered in this study. Pre-strained specimens were achieved by tensile testing system (EHF-EG250-40L) shown in Fig. 1 with the strain rate $5e-4/s$ at room temperature. The calculation equation of pre-strained value ε_{pre} is given as follows:

$$\varepsilon_{pre} = \frac{L_{pre} - L_0}{L_0} \tag{1}$$

where, L_{pre} is the initial gauge length of pre-strained specimens and L_0 is the initial gauge length of as-received specimen. Then tensile tests of as-received and pre-strained specimens were carried out with strain rate of $5e-4/s$ at room temperature. When the strain is less than 5%, the tensile strain was measured by a strain extensometer shown in Fig. 1, and when the strain is larger than the measurement range, strain was determined by the ratio of the displacement to the parallel length of specimen.

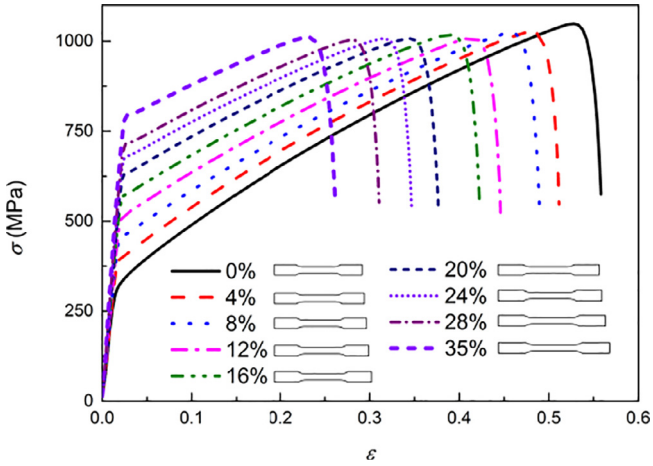

Fig. 2. Stress-strain curves of 316L austenitic stainless steel with different pre-strains.

Experimental results

Fig. 2 shows the true stress-strain (σ-ϵ) curves of 316L austenitic stainless steel with different pre-strains at room temperature. It indicates that the yield strength of 316L austenitic stainless steel increases significantly with the increase in pre-strain, but the ultimate tensile strengths of different pre-strained specimens are almost constant. Some studies also found that, the yield strength of metallic material was strengthened by pre-strain with the reduction of plasticity [21,22]. In addition, as shown in Fig. 2, stress-strain curves of 316L austenitic stainless steel can be divided into three stages: elastic stage, work hardening stage and fracture stage. With pre-strain increasing, the elastic stage is significantly enlarged, but substantial work-hardening stage is narrowed. When the stress reaches ultimate tensile strength, the specimen is necked down and fractured. The fracture strain decreases with the increase in pre-strain.

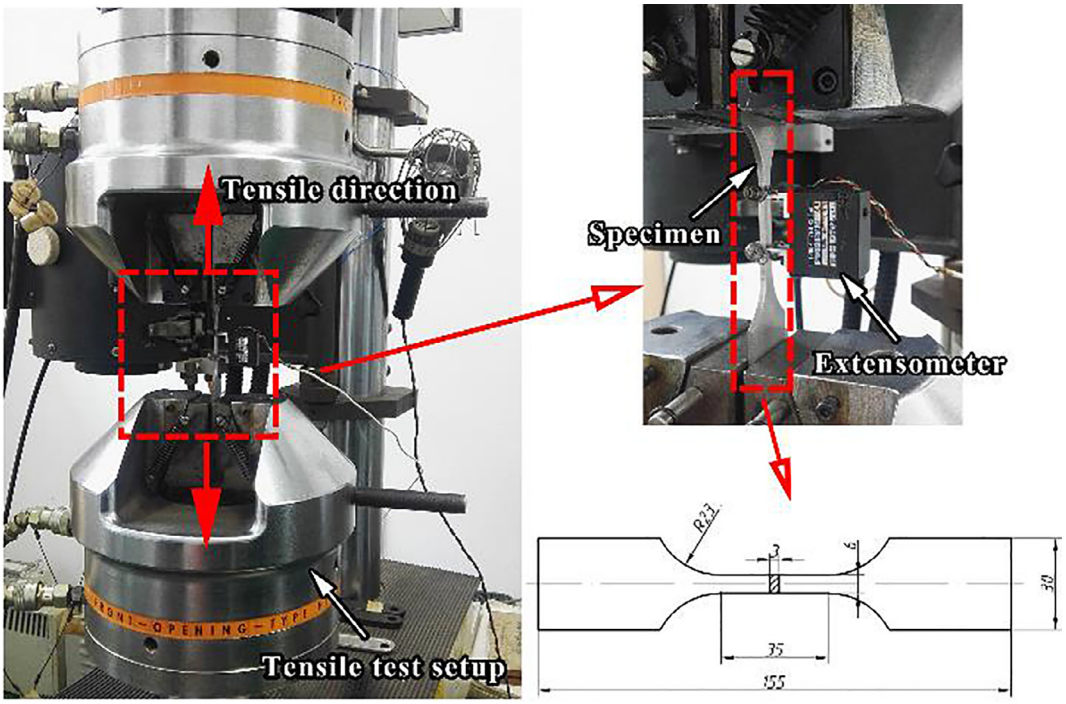

Fig. 1. Tensile test platform and tensile specimen dimensions (mm) used in this work.

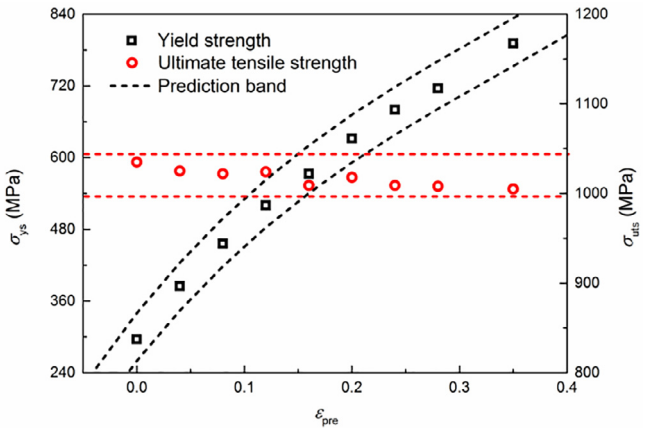

Fig. 3. Variations of yield strength and ultimate tensile strength with pre-strain.

The effect of pre-strain on mechanical behavior

The effect of pre-strain on strength parameters and plastic parameter

Fig. 3 shows the variations of strength parameters of 316L austenitic stainless steel with pre-strain. It indicates that yield strength increases obviously with the increase in pre-strain, but ultimate tensile strength is almost constant with pre-strain. For pre-strained specimens, dislocation breaks away from the pinning of solute atoms, which makes the original Kirkpatrick air mass disappear. Many studies found that pre-strain induced mechanical twinning and made dislocation multiplication [1,5,7,23,24]. Therefore, the appearances of mechanical twinning and interlaced dislocation in pre-strained specimens are the important reason for the increase in yield strength. Moreover, if the material and the experimental condition are the same, the total amount of mechanical twinning and dislocation during the experimental process are basically constant. Therefore, the ultimate tensile strengths of different pre-strained specimens are mostly constant.

Moreover, pre-strain also has a significant impact on fracture elongation of 316L austenitic stainless steel. As shown in Fig. 4, fracture elongation decreases from 65.6% to 33.6% with the increase in pre-strain from 0% to 35%. This is mainly due to the dissipation of plastic energy during pre-strained process. It also indicates that strain strengthening technology improves yield strength of 316L austenitic stainless steel by consuming plastic parameter.

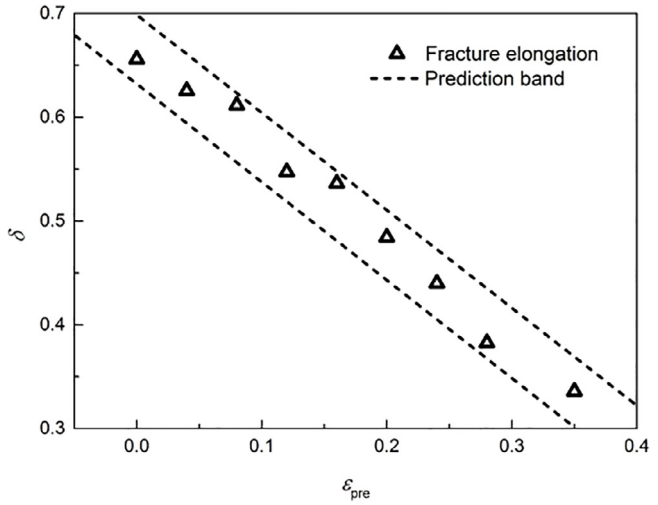

Fig. 4. Variation of fracture elongation with pre-strain for 316L austenitic stainless steel.

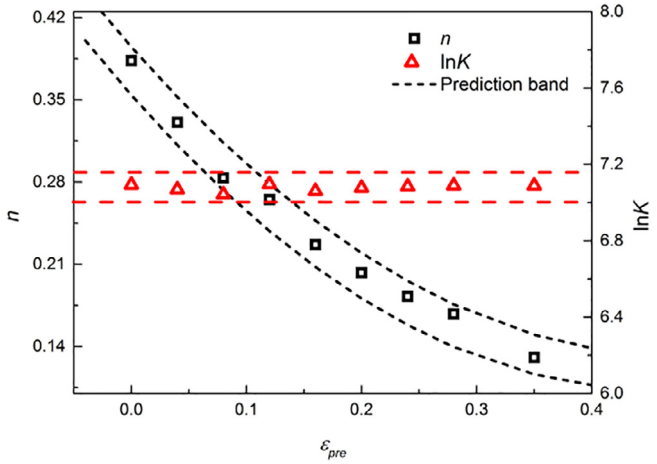

Fig. 5. Variations of strain hardening n and material constant ln$K$ with pre-strain.

The effect of pre-strain on strain hardening exponent

Hollomon model ($\sigma = K\varepsilon^n$) is used to quantitatively analyze the strain hardening behavior of materials [15–19]. $n = 1$ indicates that metallic materials are perfectly ideal elastomer, and the relationship between stress and strain is linear; $n = 0$ indicates that metallic materials do not have the capacity of strain hardening. For most metallic materials, strain hardening exponent n is 0.1–0.5 [25–28]. Taking the logarithm of Hollomon model, gives:

$$\ln\sigma = \ln K + n\ln\varepsilon \tag{2}$$

Therefore, through linear fitting of lnσ-lnε curves, the strain hardening exponent n is obtained by the fitted slopes, while the material constant ln$K$ is obtained by the fitted intercept. By this method, strain hardening exponent n and material constant K of different pre-strained specimens can be determined. Fig. 5 shows the variations of strain hardening exponent n and material constant ln$K$ of 316L austenitic stainless steel with pre-strain. It represents that strain hardening exponent n decreases with the increase in pre-strain, while material constant ln$K$ is constant for different pre-strained specimens. Due to the plasticity of austenitic stainless steel reduced by pre-strain as shown in Fig. 4, the deformation ability of austenitic stainless steel decreases with the increase in pre-strain.

The effect of energy density on mechanical behavior

The relationship between energy density and pre-strain

According to thermodynamics [29], during the pre-strain process, the work done by pulling force is transformed into kinetic energy, internal energy, and temperature increment. A finite part Σ in gauge length of the specimen is taken, the closed surface of the finite part is named S, and the surrounding volume of the finite part is named V. δW represents the work done by pulling force on the part of Σ due to the increment of tiny displacement. δU indicates that the increment of internal energy on the part of Σ due to the increment of tiny displacement. δK represents the increment of kinetic energy. δQ represents the change of heat energy. According to the first law of thermodynamics, gives:

$$\delta W = \delta K + \delta U - \delta Q \tag{3}$$

Due to the tensile tests were condicted at room temperature with the strain rate of 5e−4/s, the change of heat energy is slight during slow tensile deformation. Therefore, thermal energy and kinetic energy are negligible in this study. According to the first law of thermodynamics [29], the work by pulling force in tensile deformation is converted into

internal energy, which is stored in the specimen.

According to the above analysis, the work W done by pulling force contains two parts: one is the work W_1 done by body force X, Y and Z, the other is the work W_2 produced by surface force.

$$W_1 = \iiint_V X_i u_i dV = \iiint_V (Xu + Yv + Zw)dV \tag{4}$$

$$W_2 = \iint_s \overline{X}_i u_i dS = \iint_s (\overline{X}u + \overline{Y}v + \overline{Z}w)dS \tag{5}$$

Then:

$$W = W_1 + W_2 = \iiint_V (Xu + Yv + Zw)dV + \iint_s (\overline{X}u + \overline{Y}v + \overline{Z}w)dS \tag{6}$$

Therefore, the work done by pulling force on the part of Σ due to the increment of tiny displacement can be expressed as:

$$\delta W = \delta W_1 + \delta W_2 = \iiint_V X_i \delta u_i dV + \iint_S \overline{X}_i u_i dS \tag{7}$$

Equilibrium differential equation and static boundary condition are substituted into Eq. (7), then Eq. (8) can be acquired based on the divergence theorem:

$$\delta W = \iiint_V \sigma_{ij} \delta u_{ij} dV \tag{8}$$

Finally, the increment of internal energy increment δU is obtained as follows:

$$\delta U = \iiint_V \sigma_{ij} \delta \varepsilon_{ij} dV \tag{9}$$

The function $u_0(\varepsilon_{ij})$ is defined to satisfy the Green formula:

$$\frac{\partial u(\varepsilon_{ij})}{\partial \varepsilon_{ij}} = \sigma_{ij} \tag{10}$$

Then:

$$\delta U = \iiint_V u dV \tag{11}$$

As can be seen from Eq. (11), the function $u(\varepsilon_{ij})$ represents the strain energy density. The integral of Eq. (11) can be obtained:

$$\int_0^{u(\varepsilon_{ij})} du = u(\varepsilon_{ij}) - u(0) \tag{12}$$

where, $u(0)$ and $u(\varepsilon_{ij})$ represent the strain energy density before and after deformation, respectively. Usually, $u(0) = 0$ is taken as:

$$u(\varepsilon_{ij}) = \int_0^{\varepsilon_{ij}} \sigma_{ij} d\varepsilon_{ij} \tag{13}$$

According to the calculation method of strain energy density above, the strain energy density during tensile test is equal to the area encircled by the stress-strain curve. Fig. 6 shows the representations of elastic energy density and fracture energy density. It indicates that the elastic energy density is corresponding to the yield strength σ_y, while the fracture energy density is corresponding to the ultimate tensile strength σ_{us}. Elastic energy density presents the ability of elastic deformation, while fracture energy density controls the total deformation ability of the material. According to Eq. (13) and the results of tensile tests shown in Fig. 2, elastic energy density and fracture energy density of different pre-strained specimens can be calculated.

Fig. 7 shows the relationship between the strain energy density and pre-strain. It can be seen from Fig. 7 that elastic energy density increases with the increase in pre-strain, but fracture energy density decreases with the increase in pre-strain. It indicates that, during the pre-strain process, the energy density is rearranged. Most of the consumed fracture energy density is used to equilibrate the energy of applied load, and part of consumed fracture energy is transformed into elastic density energy.

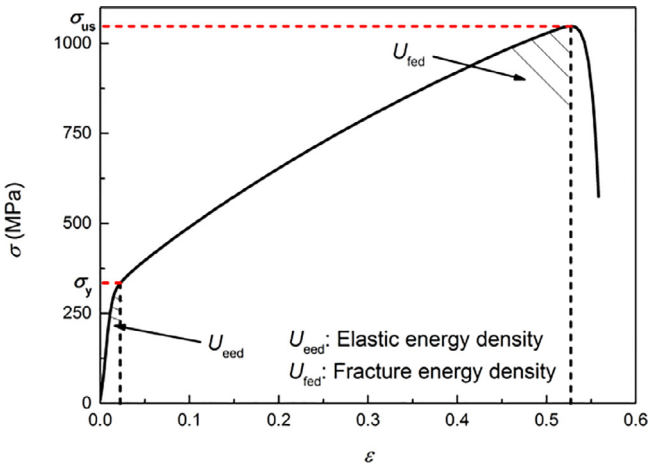

Fig. 6. Representations of elastic energy density and fracture energy density.

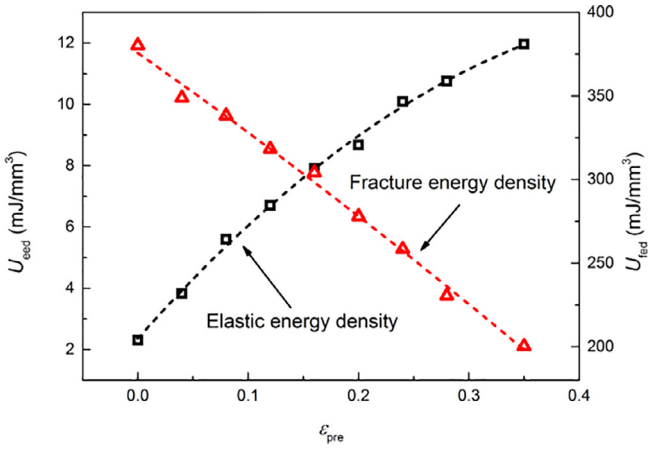

Fig. 7. Variation of energy density of 316L austenitic stainless steel with pre-strain.

Energy dissipation variable based on fracture energy density

Proposal of energy dissipation variable

Both plastic deformation and creep deformation can induce damage in metallic materials [30]. In physical phenomena, plastic damage is manifested as the formation, expansion and aggregation of holes [31]. Due to elastic modulus of metallic materials decreasing after damage, the traditional method to calculate plastic damage is to measure the damaged elastic modulus. Therefore, the damage variable can be calculated by the elastic modulus of pre-strain specimens. Using the principle of strain equivalence, it is obtained that:

$$\tilde{\sigma} = \frac{\sigma}{1-D} = E\varepsilon_e \tag{14}$$

where, $\tilde{\sigma}$ is effective stress, D is damage variable, ε_e is equivalent strain. Transposing Eq. (14) is as follows:

$$\sigma = E(1-D)\varepsilon_e = \widetilde{E}\varepsilon_e \tag{15}$$

where, $\widetilde{E}$ is elastic modulus after damage ($\widetilde{E} = \frac{\sigma}{\varepsilon_e}$). Therefore, damage variable D can be expressed as [32]:

$$D = 1 - \frac{\widetilde{E}}{E} \tag{16}$$

But there are some difficulties to accurately measure elastic modulus E. Firstly, the damage is localized and needs to be measured with a high precision strain gauge. Moreover, even in the elastic region of stress-strain curve, the nonlinearity of curve also appears, and the

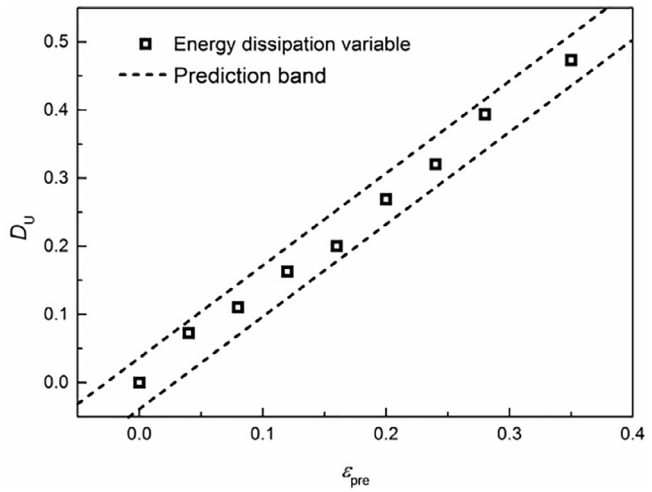

Fig. 8. Variation of energy dissipation variable D_U with pre-strain.

determination of elastic modulus is with human factor. Therefore, elastic modulus is replaced by fracture energy density to indirectly describe damage evolution of 316L austenitic stainless steel in this study. The energy dissipation variable D_U is defined as follows:

$$D_U = 1 - \frac{U_{fed\_pre}}{U_{fed\_0}} \tag{17}$$

where, U_{fed_pre} is the fracture energy density of pre-strained specimen, U_{fed_0} is the fracture energy density of as-received specimen. Fig. 8 shows the variation of energy dissipation variable D_U with pre-strain. When the material is as-received, $D_U = 0$, which indicates that the material is undamaged. With the increase in pre-strain, the energy dissipation variable D_U increases, and plastic damage appears. When $D_U = 1$, the material is totally damaged and its carrying capacity is lost. The dislocation and mechanical twinning increase with pre-strain for austenitic stainless steel, and when the pre-strain researches a critical vale, the microvoids begin to nucleate and generate in austenitic stainless steel. Therefore, the energy dissipation variable D_U increases with pre-strain value.

The effect of energy dissipation variable on mechanical properties

From the analysis of the energy dissipation variable of 316L austenitic stainless steel above, the energy dissipation variable can reveal the damage evolution of pre-strained material with pre-strain. In order to display the influence of the energy dissipation variable on the mechanical properties, Fig. 9 shows the evolutions of yield strength, ultimate tensile strength, fracture elongation and strain hardening exponent with energy dissipation variable. It shows that the yield strength increases with the increase in energy dissipation variable, but the fracture elongation and strain hardening exponent decrease with the increase in energy dissipation variable, while the ultimate tensile strength is independent on energy dissipation variable. The proposal of energy dissipation variable is based on the fracture energy density, which is a plastic damage parameter. Therefore, plastic parameters such as fracture elongation and strain hardening exponent decrease with the energy dissipation variable. On the other hand, yield strength as a strength parameter, which shows an opposite phenomenon with plastic parameter, increases with energy dissipation variable.

An improved Hollomon model based on the energy dissipation variable

Hollomon model was widely applied to describe stress-strain curve of metallic materials, and some improved Hollomon models were developed to give better results [15–19]. In classical Hollomon model, strain hardening exponent is constant with strain, which disagrees with mechanical properties of 316L austenitic stainless steel as shown in Fig. 2. Moreover, mechanical properties change significantly with pre-strain as shown in Figs. 3 and 4, which is also not considered in the classical Hollomon model. Therefore, based on energy dissipation variable, an improved Hollomon model considering the effect of pre-strain is constructed in this work. Only parts of experimental results corresponding to 0%, 8%, 16%, 24% and 35% pre-strained specimens were used to construct the constitutive model, and others were used for verification. The construction of the improved Hollomon model is as follows:

Step 1: Correlation between the parameters n and K in the improved Hollomon model with energy dissipation variable.

As shown in Fig. 5, strain hardening exponent n decreases with the increase in energy dissipation variable, while material constant K is constant. According to the analysis of energy dissipation variable mentioned above, energy dissipation variable of austenitic stainless steel and strain hardening exponent can be related as following:

$$n = A + BD_U^C \tag{18}$$

where, A, B and C are material constants, which can be fitted by partial experimental data as shown in Fig. 10(a).

Step 2: Correlation between energy dissipation variable and pre-strain.

Through the analysis of energy dissipation variables above, energy

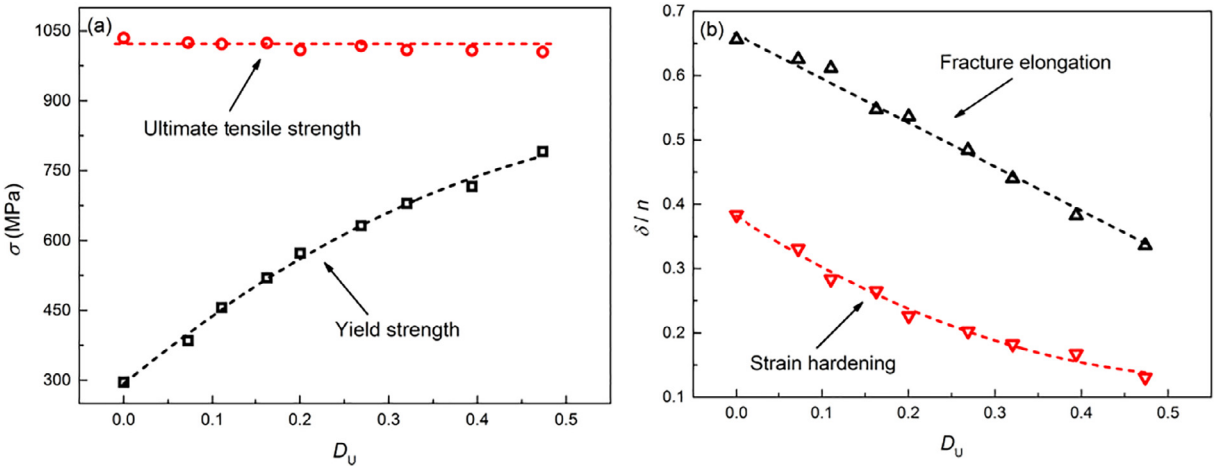

Fig. 9. The effect of energy dissipation variable on mechanical properties: (a) yield strength and ultimate tensile strength; (b) fracture elongation and strain hardening exponent.

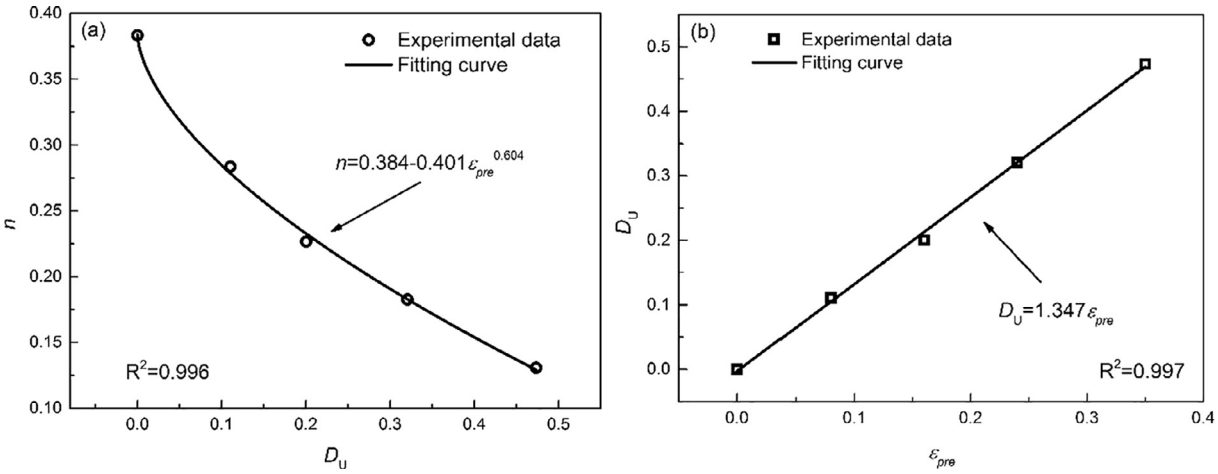

Fig. 10. Construction of the improved Hollomon model: (a) The relationship between strain hardening exponent n and energy dissipation variable D_U; (b) The relationship between energy dissipation variable D_U and pre-strain ε_{pre}.

dissipation variable and pre-strain is linear relationship, as Eq. (19):

$$D_U = k\varepsilon_{pre} \tag{19}$$

where, k is material constant, which can be fitted by partial experimental data, as shown in Fig. 10(b).

Step 3: Constructing the improved Hollomon model.

According to the above analysis, classical Hollomon model is improved as the following form:

$$\begin{cases} \sigma = K\varepsilon^{A+BD_U^C} \\ D_U = k\varepsilon_{pre} \end{cases} \tag{20}$$

This improved Hollomon model is based on the energy dissipation variable, and the damage process caused by pre-strain is considered in this model. According to experimental data analysis of 316L austenitic stainless steel, the improved Hollomon model can be obtained as Eq. (21).

$$\begin{cases} \sigma = K\varepsilon^{0.384-0.401\cdot D_U^{0.604}} \\ D_U = 1.347\cdot\varepsilon_{pre} \end{cases} \tag{21}$$

The improved Hollomon model has the following advantages: (1) Classical Hollomon model only considers the effect of strain hardening behavior, but the improved Hollomon model considers the influence of the energy dissipation variable on mechanical behavior with physical meaning; (2) The improved Hollomon model takes account of the effect of pre-strain, and it can predict stress-strain curves of different pre-strained specimens.

In order to verify this improved Hollomon model, other four sets of experimental data are used to verify the predicted values by the improved Hollomon model shown in Fig. 11. It suggests that the stress-strain curves predicted by the improved Hollomon model agree well with the experimental results for different pre-strained specimens.

Correlation coefficient R provides information on the strength of linear relationship between experimental data and predicted data [33]. The calculation equation of R is given as:

$$R = \frac{\sum_{i=1}^{N}(E_i-\overline{E})(P_i-\overline{P})}{\sqrt{\sum_{i=1}^{N}(E_i-\overline{E})^2\sum_{i=1}^{N}(P_i-\overline{P})^2}} \tag{22}$$

where, E_i is the experimental data and P_i is the predicted data, $\overline{P}$ and $\overline{E}$ are mean values of P and E, respectively. N is the total number of data employed in the investigation.

Fig. 12 shows the correlations of experimental data and predicted values by improved Hollomon model of the whole experimental data. It can be seen that most of data points agree well, and the correlation coefficients is 0.9944. It indicates that the improved Hollomon model considering the energy dissipation variable during pre-strain process is suitable to describe mechanical behavior of different pre-strained specimens.

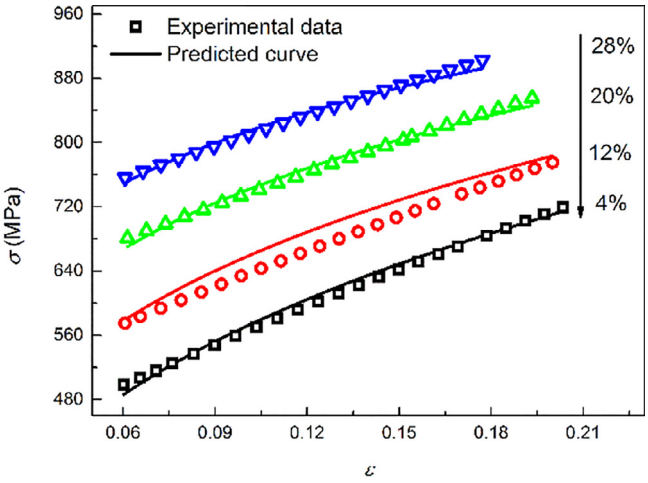

Fig. 11. Comparison between the experimental data and predicted results by improved Hollomon model for the other four pre-strained specimens.

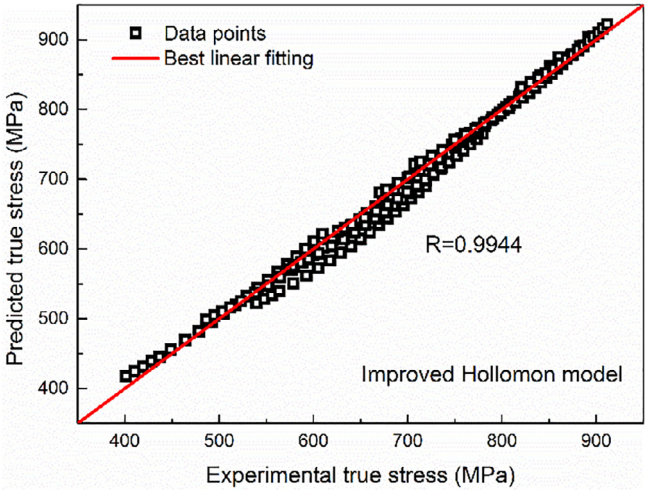

Fig. 12. Correlation between experimental data and predicted results by improved Hollomon model for different pre-strained specimens.

Conclusion

The effect of pre-strain on mechanical properties of 316L austenitic stainless steel was investigated in this work. Yield strength increases from 296 MPa to 791 MPa and fracture elongation decreases from 0.656 to 0.336 with the increase in pre-strain from 0% to 35%. But ultimate tensile strength is basically constant as 1025 MPa. An energy dissipation variable was proposed based on fracture energy density, and the effect of the energy dissipation variable on tensile behavior of pre-strained 316L austenitic stainless steel was analyzed. Yield strength increases with the increase in energy dissipation variable, but strain hardening exponent and fracture elongation decrease with the increase in energy dissipation. Finally, based on energy dissipation variable, an improved Hollomon model considering the effect of pre-strain was developed in this study, and can be applied for pre-strained 316L austenitic stainless steel with acceptable accuracy.

Acknowledgement

This work was supported by the National Natural Science Foundation of China [grant numbers 51505041]; the Natural Science Foundation of the Jiangsu Higher Education Institutions of China [grant numbers 16KJB460002].

Appendix A. Supplementary data

Supplementary data associated with this article can be found, in the online version, at http://dx.doi.org/10.1016/j.rinp.2018.05.034.

References

[1] Lee WS, Lin CF. Effects of pre-strain and strain rate on dynamic deformation characteristics of 304L stainless steel: part 2 – Microstructural study. Mater Sci Technol 2002;18(8):877–84.
[2] Choi BG, Jo CY, Hong HU, Kim IS, Kim HM. Effect of pre-strain on microstructural evolution during thermal exposure of single crystal superalloy CMSX-4. Trans Nonferrous Metals Soc China 2011;21(6):1291–6.
[3] Quan LW, Zhao G, Gao S, Muddle BC. Effect of pre-stretching on microstructure of aged 2524 aluminium alloy. Trans Nonferrous Metals Soc China 2011;21(9):1957–62.
[4] Wang Y, Wang X, Gong J, Shen L, Dong W. Hydrogen embrittlement of catholically hydrogen-precharged 304L austenitic stainless steel: Effect of plastic pre-strain. Int J Hydrogen Energy 2014;39(25):13909–18.
[5] Ji H, Park IJ, Lee SM, Lee YK. The effect of pre-strain on hydrogen embrittlement in 310S stainless steel. J Alloy Compd 2014;598(3):205–12.
[6] Park IJ, Jung JG, Jo SY, Lee SM, Lee YK. The effect of pre-strain on the resistance to hydrogen embrittlement in 316L Austenitic Stainless Steel. Mater Trans 2014;55(6):964–70.
[7] Peng Y, Gong J, Jiang Y, Fu M, Rong D. The effect of plastic pre-strain on low-temperature surface carburization of AISI 304 austenitic stainless steel. Surf Coat Technol 2016;304:16–22.
[8] Peng J, Li KS, Peng J, Pei JF, Zhou CY. The effect of pre-strain on tensile behaviour of 316L austenitic stainless steel. Mater Sci Technol 2018;34(5):547–60.
[9] Gbenebor OP, Fayomi OSI, Popoola API, Inegbenebor AO, Oyawale F. Extrusion die geometry effects on the energy absorbing properties and deformation response of 6063-type Al–Mg–Si aluminum alloy. Results Phys 2013;3:1–6.
[10] Lazzarin P, Zambardi R. The Equivalent Strain Energy Density approach re-formulated and applied to sharp V-shaped notches under localized and generalized plasticity. Fatigue Fract Eng Mater Struct 2002;25:917–28.
[11] Koh SK. Fatigue damage evaluation of a high pressure tube steel using cyclic strain energy density. Int J Press Vessels Pip 2002;79(12):791–8.
[12] Lazzarin P, Berto F, Gomez FJ, Zappalorto M. Some advantages derived from the use of the strain energy density over a control volume in fatigue strength assessments of welded joints. Int J Fatigue 2008;30(8):1345–57.
[13] Guu YH, Hocheng H, Chou CY, Deng CS. Effect of electrical discharge machining on surface characteristics and machining damage of AISI D2 tool steel. Mater Sci Eng, A 2003;358(1–2):37–43.
[14] Nagode M, Šeruga D. Fatigue life prediction using multiaxial energy calculations with the mean stress effect to predict failure of linear and nonlinear elastic solids. Results Phys 2016;6:352–64.
[15] Hollomon JH, Member J. Tensile deformation. Metals Technol 1945;12:268–90.
[16] Zhang SC, Zheng WJ, Song ZG, Feng H, Sun Y. Effect of cold deformation on structure and mechanical behavior of Inconel 690 Alloy. J Iron Steel Res 2009;21(12):49–54.
[17] Colla V, Sanctis MD, Dimatteo A, Lovicu G, Solina A, Valentini R. strain hardening behavior of dual-phase steels. Metall Mater Trans A 2009;40(11):2557–67.
[18] Hertelé S, Waele WD, Denys R. A generic stress–strain model for metallic materials with two-stage strain hardening behavior. Int J Non Linear Mech 2011;46(3):519–31.
[19] Peng J, Zhou CY, Dai Q, He XH, Tang ZX, Du YQ. The strain rate sensitivity of commercial purity titanium at room temperature and the improvement of Hollomon empirical formula. Rare Metal Mater Eng 2013;42(3):483–7.
[20] ASTM E8M-04, Standard Test Methods for Tension Testing of Metallic Materials.
[21] Feng XS, Qian CF, Chen ZW, Yang TC. Light-weight design of cryogenic storage tank based on strain-strengthening Technology. Pressure Vessel Technol 2011.
[22] Zheng JY, Li YX, Xu P, Ma L, Miao CJ. Influence factors of mechanical property for strain strengthening austenitic stainless steel. J PLA Univ Sci Technol 2011;12(5):512–9.
[23] Eskandari M, Najafizadeh A, Kermanpur A. Effect of strain-induced martensite on the formation of nanocrystalline 316L stainless steel after cold rolling and annealing. Mater Sci Eng, A 2009;519(1–2):46–50.
[24] Shen YF, Li XX, Sun X, Wang YD, Zuo L. Twinning and martensite in a 304 austenitic stainless steel. Mater Sci Eng, A 2012;552(34):514–22.
[25] Hosford WF. Mechanical behavior of materials. New York: Cambridge University Press; 2005.
[26] Byun TS, Hashimoto N, Farrell K. Temperature dependence of strain hardening and plastic instability behaviors in austenitic stainless steels. Acta Mater 2004;52(13):3889–99.
[27] Dini G, Najafizadeh A, Ueji R, Monir-Vaghefi SM. Tensile deformation behavior of high manganese austenitic steel: the role of grain size. Mater Des 2010;31(7):3395–402.
[28] Yang X, Wang X, Ling X, Wang D. Enhanced mechanical behaviors of gradient nano-grained austenite stainless steel by means of ultrasonic impact treatment. Results Phys 2017;7.
[29] Gaskell DR, Laughlin DE. Introduction to the thermodynamics of materials. 6th ed. New York: Tylor & Francis; 2017.
[30] Zhang YC, Jiang W, Tu ST, Zhang XC, Ye YJ. Creep crack growth behavior analysis of the 9Cr-1Mo steel by a modified creep-damage model. Mater Sci Eng, A 2017;708.
[31] Tanguy B, Luu TT, Perrin G, Pineau A, Besson J. Plastic and damage behaviour of a high strength X100 pipeline steel: Experiments and modelling. Int J Press Vessels Pip 2008;85(5):322–35.
[32] Mashayekhi M, Ziaei-Rad S. Identification and validation of a ductile damage model for A533 steel. J Mater Process Tech 2006;177(1–3):291–5.
[33] Lin YC, Nong FQ, Chen XM, Chen DD, Chen MS. Microstructural evolution and constitutive models to predict hot deformation behaviors of a nickel-based superalloy. Vacuum 2017;137:104–14.